ATLAS NOTE

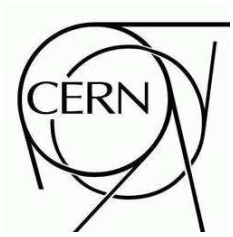

Response of the ATLAS Tile Calorimeter to Hadrons in Stand-Alone Testbeam Data

T. Davidek[1)], M. Volpi[2)], T. Zenis[3)]

[1)] Charles University in Prague, Faculty of Mathematics and Physics, Institute of Particle and Nuclear Physics, Czech Republic

[2)] Institut de Fisica d'Altes Energies, Universitat Autònoma de Barcelona, Barcelona, Spain

[3)] Comenius University, Bratislava, Slovakia

ATL-TILECAL-PUB-2009-004
13 March 2009

Abstract

Several Tilecal modules were exposed to hadron beams in the H8 SPS area. This note describes the pion response studies performed on data acquired during five testbeam periods. Analyzed data were reprocessed to account for the new calibration as described in another Tilecal note [1]. Results on uniformity of the response across modules at a fixed pseudorapidity and within a module over the full range of pseudorapidity are presented. The pion response and energy resolution as a function of beam energy ranging from 10 GeV to 350 GeV is then addressed.

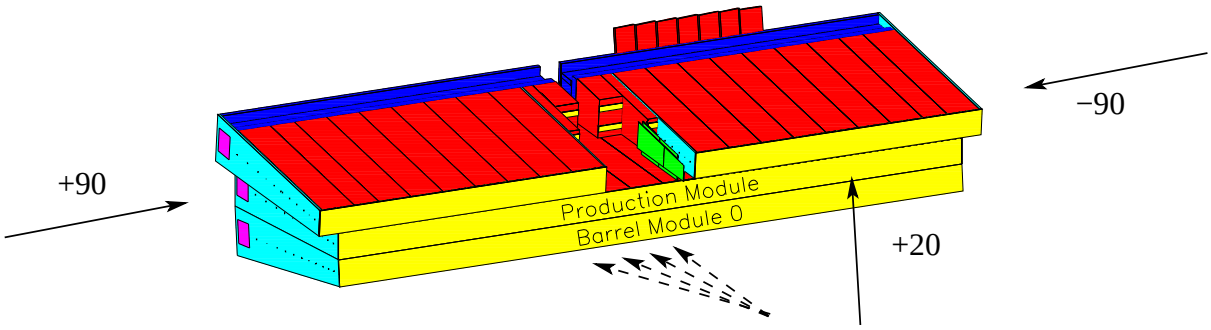

Figure 1: The typical testbeam setup with barrel module 0 placed at the bottom, production barrel module in the middle and two production extended barrel modules on the top of the module stack. The arrows indicate the beam directions.

1 Introduction

The Tilecal production modules were extensively tested with particle beams in SPS H8 zone over four consecutive years 2000–2003. After the Tilecal calibration on EM scale has been better understood [1], data from several testbeam periods 2002–2003 were re-processed to reflect all improvements. In this note we present the analyses of the modules response to hadrons, performed on the re-processed data. Understanding the calorimeter response to single hadrons is an important step towards precise calorimeter measurements in the ATLAS detector.

During the testbeam periods data were recorded with electrons, muons and hadrons covering the energy range from 10 GeV to 350 GeV. Tilecal modules under test were placed on the scanning table capable of placing modules at any desired position and angles with respect to the incoming particles. Thus beams impinged the calorimeter modules at various impact points and angles. A typical testbeam setup is shown in Fig. 1.

The beamline was equipped with three beam scintillators S1, S2, S3 and two x-y delay wire chambers upstream of the calorimeter modules. The scintillator counters defined the trigger and the beam chambers were used to measure the beam position. A pair of Cherenkov counters was also installed to assist in particle identification.

Tile calorimeter uses four calibration systems:

- Cs system measures the response of individual tiles to Cs radioactive source. This system calibrates optical components (tiles, fibers) as well as the photomultipliers (PMTs).
- Minimum bias system is designed to monitor the response of each Tilecal cell to minimum-bias interactions during the physics data taking.
- Charge injection system (CIS) injects a well-defined charge into the bi-gain fast readout electronics and provides the conversion factor ADC-to-charge in every readout channel. Moreover, it provides appropriate corrections that restore the linearity of the response in low-gain [2].
- Laser system monitors the PMT stability and provides eventual corrections for the PMT non-linearity.

Whereas the first two systems use the slow integrator readout, CIS and laser are readout by the fast electronics as the physics events are.

Only the Cs system and CIS calibrations were used to calibrate the Tilecal response to EM scale in testbeams. The response of individual PMTs is equalized with Cs source prior to data taking in every testbeam period. At the same time, the fast readout electronics is calibrated with CIS. The overall EM scale is then determined using electrons impinging the calorimeter modules at 20°. Corrections are applied in second and third radial calorimeter compartments to ensure the uniform EM scale across the whole calorimeter [1].

The analyzed data were recorded during five testbeam period, see Appendix A for more details. The list of bad channels is also given there for reference.

2 Data selection

The beams in SPS H8 zone are usually a mixture of electrons, muons and hadrons. Several selection criteria have been applied to the studied data samples in order to select appropriate particle type with the correct energy. The following cuts have been used:

- Only physics events (Trig=1) without digital data corruption are accepted.
- Signal in beam counters S1 and S3 is required to be compatible with that of a single minimum ionizing particle. This cut avoids events with upstream energy loss and also double-particle events.
- Events with large angle with respect to beam axis as well as off-axis events have potentially incorrect energy. Such events are therefore removed from the data samples using information from the beam chambers.
- In-time events are selected by requiring the reconstructed time in low-gain channels (Tfit) to be in the range $(-60, 60)$ ns.
- The signal amplitude in low-gain channels is required to be larger than 10 pC.[1)] By imposing this condition one avoids events with mis-measured energy in the calorimeter; these are typically small signals, but the electronics switched to low-gain due to large undershoot in high-gain.
- Muons are removed by cutting out events with very low energy deposits in all radial calorimeter compartments.

The share of different particle types in the beam depends on the beam element settings. While electron beams contain electrons, muons and hadrons, the nominal hadron beams contain only muons and hadrons. This is demonstrated in Fig. 2. For energies $E_{\text{beam}} > 20$ GeV a special check for the presence of electrons has been carried out using the electron selection criteria (see Section 2.1).

2.1 Electron/hadron separation

The electron/hadrons separation is based on the different size of the electromagnetic and hadronic showers in the calorimeter. The quantity called *average density* (AvD) [3] is used for this purpose. It is

[1)] Note that the switch from high-gain to low-gain occurs typically at 12 pC.

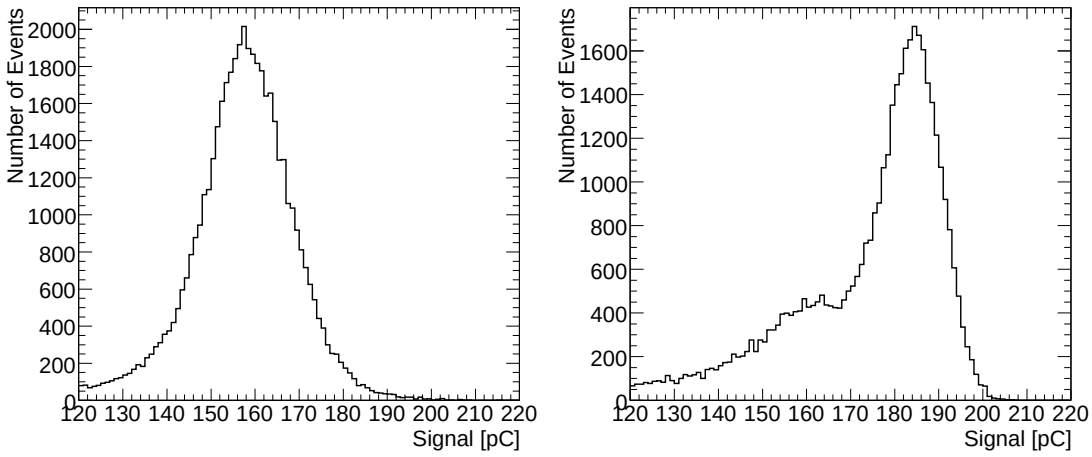

Figure 2: The response of the Tilecal modules to 180 GeV hadron (left) and electron (right) beams. Electron beam contains both electrons (peak at 185 pC) and hadrons (peak at 160 pC); hadron beam consists of only hadrons.

defined

$$\mathrm{AvD} = \frac{1}{N_{\mathrm{cell}}} \sum_{i \in \mathrm{cells}}^{S_i > \mathrm{thr}} \frac{S_i}{V_i} \tag{1}$$

where S_i is signal of i^{th}, V_i represents the volume of i^{th} cell and N_{cell} is the number of cells above the threshold. The threshold for a cell signal of 0.06 pC is used. In addition, only cells inside 3×3 towers around the beam impact point are used. The AvD spectra for 180 GeV electrons and hadrons are showed in Fig. 3 as an example.

Actual value of the AvD cut depends on the incident energy and also varies with pseudorapidity. For instance, the condition $\mathrm{AvD} < 0.6\ \mathrm{pC/dm^3}$ was used separate hadrons from electrons from the 180 GeV nominal electron beam entering the calorimeter modules at $\eta = 0.35$ (see also Fig. 2).

For nominal energies $E_{\mathrm{beam}} \geq 50$ GeV, the average density provides a clean tool for electron/hadron separation. After applying the AvD, the residual electron contamination is below 0.1 %. For nominal electron beams with $E_{\mathrm{beam}} \leq 20$ GeV the average density is not sufficient for good electron/hadron separation.[2)] Cherenkov signal is therefore used to improve the separation; the resulting performance of the separation procedure is similar to that for higher energies mentioned above.

2.2 Pion/proton separation

The positively charged beams ($50 - 180$ GeV) contain not only pions but also a significant fraction of protons. Since pions and protons have very similar calorimeter response (see e.g. Fig. 4), they cannot be separated by calorimeter signal criteria. Instead, the Cherenkov counter is used to select pions in such cases. Typically, Cherenkov counter is set to medium pressure below proton threshold, while it still provides high efficiency for pions. The Cherenkov counter signal is shown in Fig. 5 for the two extreme beam energies as an example.

[2)] At low energies, the rather coarse cell segmentation in Tilecal causes the worse performance of AvD.

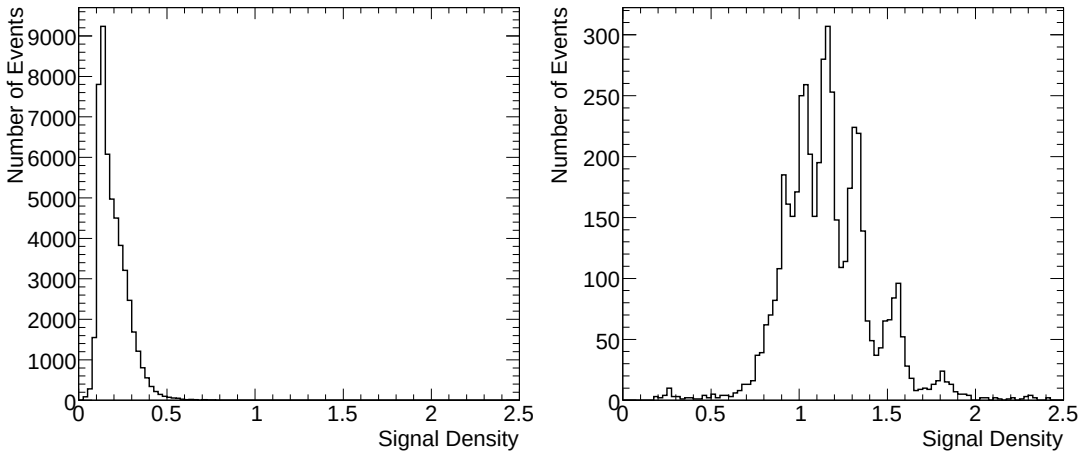

Figure 3: The average density (AvD) of the signal from 180 GeV hadrons (left) and electrons (right) impinging the calorimeter at $\eta = 0.35$. AvD is displayed in units of pC/dm^3. The multiple peak structure seen for electrons is due to different N_{cell} in different events. Electrons are selected by requiring total signal over 190 pC (see also Fig. 2).

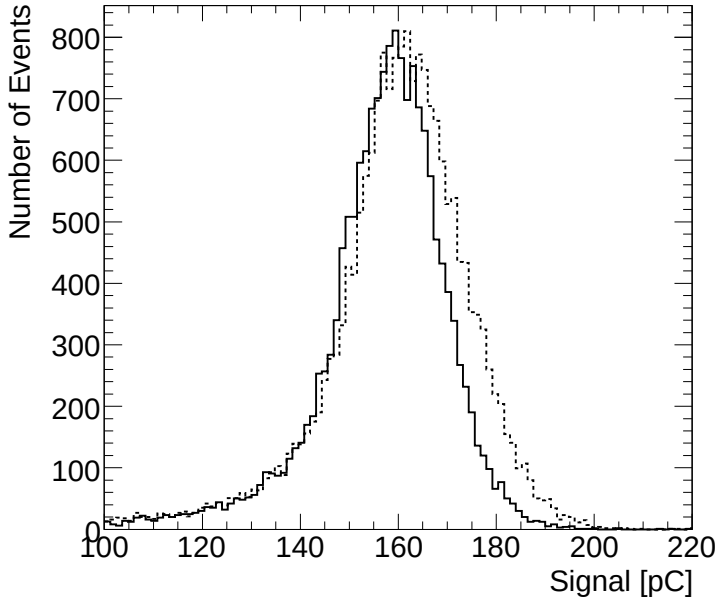

Figure 4: Comparison of the Tilecal response to 180 GeV protons (full line histogram) and pions (dashed line histogram). Particles were separated using the Cherenkov signal.

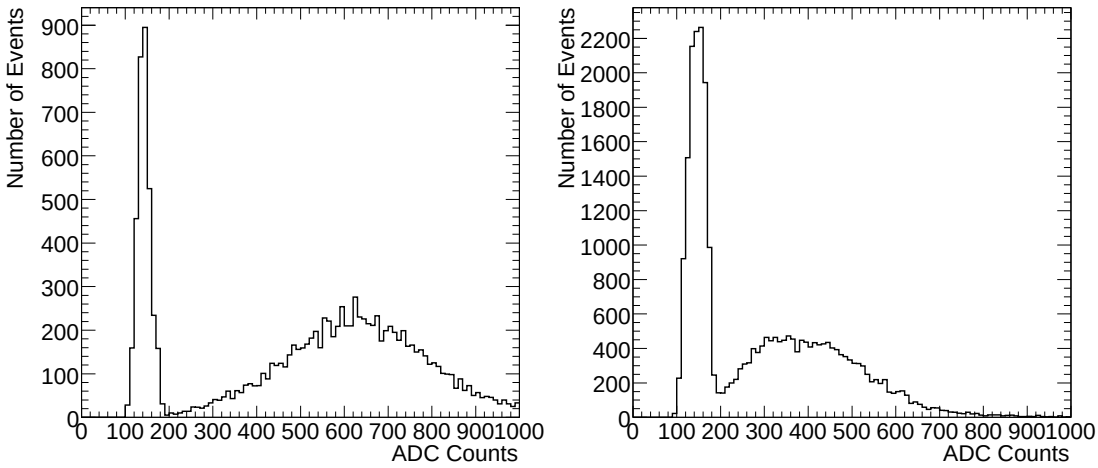

Figure 5: The response of the Cherenkov counter for 50 (left) and 180 GeV (right) positive hadron beams. The narrow peaks compatible with pedestal correspond to proton, shoulders on the right represent pions.

The pion/proton separation has been verified by comparing the ratio n_1/n_0 of particles not interacting in the first radial calorimeter compartment to the total number of incoming particles, separately for pions and protons as selected by the Cherenkov counter signal. This ratio depends on the length l of the first calorimeter compartment as seen by the beam and on the respective interaction length $\lambda_{\rm I}$

$$n_1/n_0 = \exp\left(\frac{-l}{\lambda_{\rm I}}\right) \tag{2}$$

The relation between interaction length for protons and pions is [4]:

$$\lambda_{\rm I}^{\pi} = 1.22\,\lambda_{\rm I}^{p} \tag{3}$$

From Eqs. (2) and (3) we get:

$$\left.\frac{n_1}{n_0}\right|_p = \left(\left.\frac{n_1}{n_0}\right|_\pi\right)^{1.22} \tag{4}$$

The number of particles passing the first calorimeter compartment without hadron interaction n_1 is calculated from total area of the Landau⊗Gauss convolution fitted on the signal distribution of the first radial calorimeter compartment. The fitted function corresponds to the signal from a minimum ionizing particle, the fit is performed in the range of from -0.2 to 1 pC.[3)]

The ratio n_1/n_0 for pions and protons entering the calorimeter at $|\eta| = 0.35$ is shown in Fig. 6. For each run three symbols are displayed:

- Events with Cherenkov counter response above the pedestal; these events are expected to be pure pions.
- Events with Cherenkov counter compatible with pedestal; these are protons with pion contamination due to non-100 % efficiency of the Cherenkov counter.
- Expected ratio n_1/n_0 for protons calculated from the number of selected pions using the formula (4).

[3)] This procedure for evaluating the the total number of events with no hadron interaction was also tested with muons.

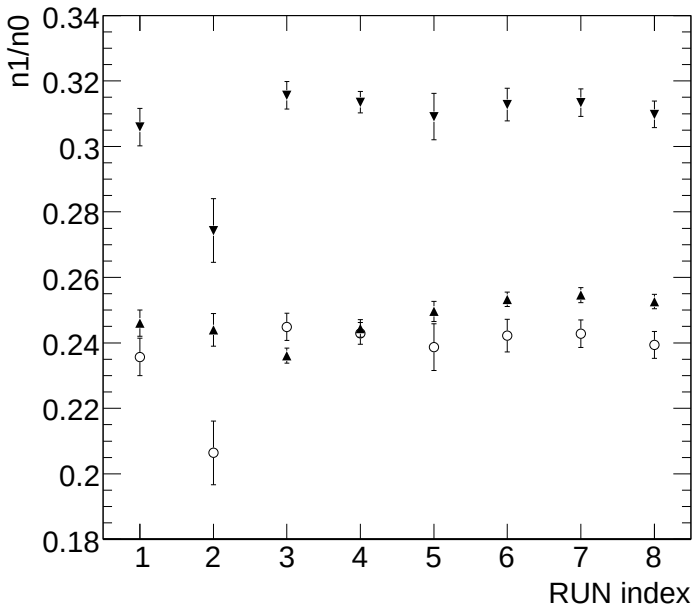

Figure 6: Ratio n_1/n_0 of events without hadronic interaction in the first radial Tilecal compartment and all events. Data were taken with 100 GeV (run index 1, 2 corresponding to runs 210319, 340487) and 180 GeV (run index ≥ 3, runs 200225, 200237, 200416, 210398, 340427, 340436) hadron beams during various testbeam periods. Full down (up) triangles correspond to Cherenkov-selected pions (protons), the open circles represent the expected ratio for protons as calculated with the formula (4). All errors shown are statistical.

The ratio n_1/n_0 for selected pions (full down triangle) is constant for all runs except of run 340487 (100 GeV, July 2003 testbeam period). Since the expected ratio n_1/n_0 of protons matches reasonably well the measured one, the pion/proton separation based on Cherenkov counter works well.

3 Signal reconstruction

The signal from each PMT is reconstructed using the fit method. The total calorimeter signal is summed from all cells within a 3×3 tower matrix, where each tower spans $\Delta\eta \times \Delta\phi = 0.1 \times 0.1$. The matrix is centered on the cell hit by the beam and corresponds to a cone of a radius $R \approx 0.2$, see Appendix B for more details. This energy sum is systematically smaller than that of all cells of all modules in a stack. Therefore, an appropriate transverse leakage correction is applied to the measured mean response in Section 5.2. No correction is needed for the energy resolution, that is observed to be almost entirely independent of the energy summing method.[4)]

Hadron energies are reconstructed at the EM scale, using one global calibration factor 1.05 pC/GeV and applying the weights in the individual radial calorimeter compartments [1].

The results described in Section 5 deal with the mean response. It is defined as the Gaussian peak

[4)] Other methods have been tested as well: summing all calorimeter cells with a signal above threshold determined by the noise width and summing all calorimeter cells unconditionally. The latter method suffers also from the non-Gaussian noise in the channels close to the patch-panel; these channels are typically far away from the cells hit by the beam.

value fitted on the signal spectrum in the $\pm 2\sigma$ range. Technically, a 100 channel histogram is created in the range of mean $\pm$ 5σ and then filled with the 3×3 tower signals. The Gaussian fit is then iteratively applied until the convergence in the peak value and σ is reached.

4 Beam energy corrections

Data were taken at various nominal beam energies. Nevertheless, the corrections were calculated using the known settings of the bending magnets and collimators in the beamline for every run [5]. The corrected beam energies are taken into account in studies of pion response and energy resolution as a function of beam energy (Sections 5.2, 5.3). The systematic uncertainty in the beam energy associated with the uncertainties in the magnet currents were calculated as well. This uncertainty then contributes to the total uncertainty in the pion response relative to the beam energy, see Section 5.2.

5 Results

The experimental results are addressed in this Section. First, we report the uniformity studies at a fixed energy. Then the pion response and the energy resolution measured at a fixed angle are given, both as a function of the incident energy.

Basically all data available from five testbeam periods (see Appendix A) relevant for the above mentioned issues were studied. Only excluded were runs where a cell within the 3*x*3 tower matrix suffered from non-recoverable problems, typically when both PMTs in such cell were not working. Altogether, about 25 runs were analyzed. In addition few special runs were investigated in order to assess the noise contribution.

Experimental results are also compared to GEANT4 MC simulations [6], version 8.3. Hadronic interactions are simulated with the Quark Gluon String Precompound (QGSP) and Bertini intranuclear cascade models [7].

5.1 Response uniformity

Since most of the Tilecal modules were exposed to positive polarity beam of 180 GeV, the uniformity of the response was investigated using these data. However, the Cherenkov counter was not always operational. In order to maximize the data set for studying the module uniformity, no pion/proton separation was performed. Therefore, we refer to this data set as to hadrons.

The response uniformity within one module was investigated with 180 GeV hadrons. The response and the fractional energy resolution as a function of pseudorapidity are shown in Fig. 7. These results were obtained with a setup in which a production barrel module was placed above the central barrel module instead of the two extended barrel modules. This eliminated the transverse leakage present in the usual setup (see Fig. 1) for incidence at small pseudorapidities.

The mean response in Fig. 7, left is slightly lower for small pseudorapidities due to longitudinal leakage from the back of the calorimeter modules. The responses corrected for this effect are also shown in the figure, while more details are given in Appendix C. The lower response at $|\eta| = 0.75$ is due

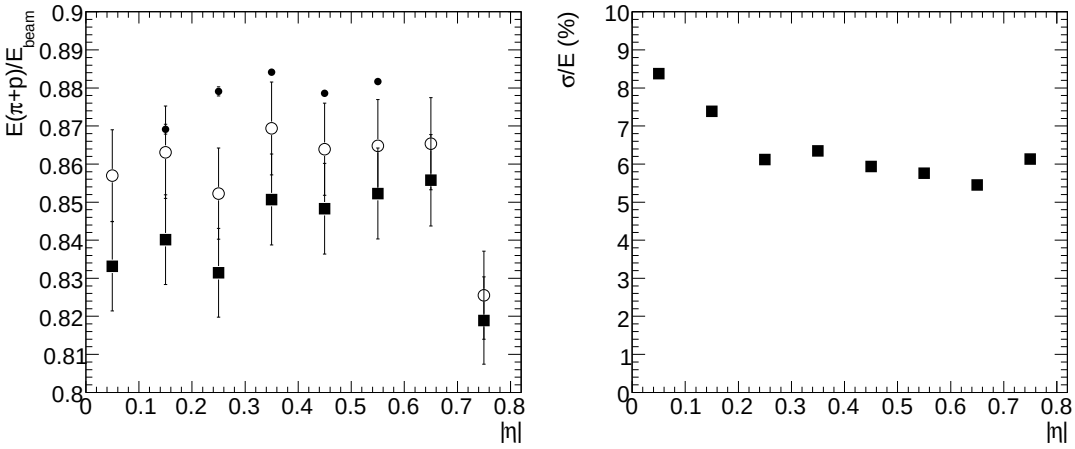

Figure 7: The mean reconstructed energy (left) and resolution (right) for 180 GeV hadrons incident at various pseudorapidities. Full squares denote the data. The open and small full circles represent data and GEANT4 MC simulations (given only in the range $0.15 \leq |\eta| \leq 0.55$) respectively, after applying the longitudinal leakage corrections (see Appendix C).

to transverse leakage from the side of modules. Excluding the latter point, the response corrected for longitudinal leakage has an RMS spread of 0.61 ± 0.16 %.

The energy resolution as a function of pseudorapidity is shown in Fig. 7, right panel. As expected, it is significantly worse where longitudinal leakage is larger, but it appears to be only insignificantly affected by transverse leakage at $|\eta| = 0.75$.

The module-to-module uniformity was studied with 180 GeV hadrons entering the calorimeter at $|\eta| = 0.35$. The data set comprises eight runs, each taken in the setup with different central barrel module on the scanning table. The results are shown in Fig. 8. The RMS spread amounts to (1.6 ± 0.4) %. It should be noted that one of the entries corresponds to testbeam setup with 3 barrel modules in the stack. Excluding this point, the resulting RMS spread is (1.4 ± 0.4) %.

The obtained RMS spread is compatible with the results of earlier analysis performed on data with older calibration:[5)] this data set involved nine modules, the RMS spread was (1.5 ± 0.4) % [8].

5.1.1 Understanding the response variation

As has been shown in previous Section, the pion response varies module-to-module as well as within one module as a function of pseudorapidity. Several sources affect the resulting spread of the pion response:

- Local variations in the Tilecal optics system, involving the differences in the light yields of the tiles, nonuniformity of light collection within the tiles, variations in the tile-to-fiber optical couplings etc [1]. These variations are mapped with Cs source and their impact on the total pion response has been evaluated with special MC simulation where all individual tile and fiber responses are taken into account.

[5)] Cesium calibration with integral method, original CIS calibration with no correction for non-linearity in the low-gain, no corrections for EM scale in individual radial compartments as defined in Ref. [1].

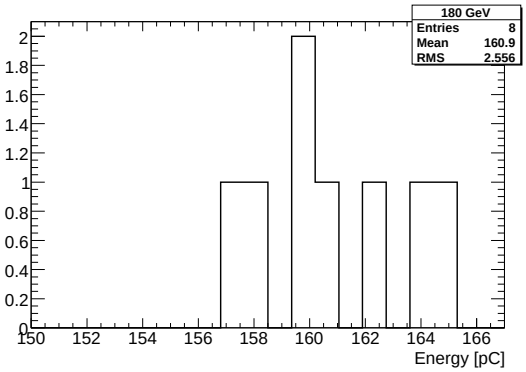

Figure 8: The module-to-module uniformity for 180 GeV pions incident at $|\eta| = 0.35$ in the Each entry corresponds to different central barrel module. The RMS spread amounts to $(1.6 \pm 0.4)\,\%$.

- Uncertainty associated with the individual electronic channel calibration, as determined with the charge injection system [2].
- Uncertainty in the gain of individual PMT. Although the gain of all PMTs is equalized with Cs source in the beginning of every testbeam period, subsequent Cs scans taken usually in the end of the testbeam period show the typical RMS spread of 0.5 %.
- Uncertainty in the global EM scale of the given Tilecal module due to Cs calibration procedure. This procedure relies on the integrator calibration, which however was not systematically measured during the testbeam periods. The biggest uncertainty (at the level of 0.6 %) comes from the integrating ADC; since there is one such ADC per superdrawer, it affects the overall EM scale in a module.

In the following text, we shall compare the observed pion response variation with uncertainties in the calibration of individual Tilecal components.

Uniformity within a module

- The impact of the local variations in the optics system on the resulting response of 180 GeV hadrons was found with special MC simulation mentioned above and amounts to $0.4 - 0.5\,\%$. Note that this is much smaller than for electrons [1], since hadron showers spread over significantly bigger volume in the calorimeter than electrons and most of the local variations average out.
- Studies reported in Ref. [2] predict an RMS spread of 0.43 % for 180 GeV hadrons due to uncertainties associated with the fast readout electronics.[6)]
- The variation in the PMT gain of 0.5 % has negligible impact on the resulting hadron response, since many channels are involved.
- The uncertainty in the global EM scale does not contribute in this case, since all experimental data were acquired within one module.

[6)] Strictly speaking, the experimental results obtained at individual pseudorapidities are not entirely independent as far as the readout electronics calibration is concerned, since hadronic showers spread over more than 1 tower in $\eta \times \phi = 0.1 \times 0.1$. Therefore, the above number represents an upper limit in this particular case. On the other hand, the major contribution comes from the central tower hit by the beam, where 180 GeV hadrons deposit most of their energy.

Run	Central Barrel Module	Response (pC)	Average integrator gain (MΩ)
220130	JINR01, C-side	162.40 ± 0.14	28.62 ± 0.02
330176	JINR12, C-side	158.42 ± 0.12	29.11 ± 0.02
330189	JINR12, A-side	160.68 ± 0.13	28.90 ± 0.02
340168	JINR27, C-side	159.43 ± 0.17	29.02 ± 0.02
340148	JINR27, A-side	157.07 ± 0.14	28.90 ± 0.02

Table 1: The response to 180 GeV hadrons entering the calorimeter at $|\eta| = 0.35$ along with the integrator calibration not yet applied to the data. Results are shown only for modules where the integrator calibration is known. All errors are statistical only.

The total predicted RMS spread amounts to $\sim 0.65\,\%$ (individual contributions listed above are summed in quadrature). This is in a good agreement with the experimental value of $(0.61 \pm 0.16)\,\%$ obtained after correcting the response for longitudinal energy leakage.

Uniformity across modules In order to compare the measured spread with that expected from the individual uncertainties mentioned above, the analysis was restricted to 5 modules where the integrator calibration could be recovered. The results are given in Table 1. The experimental data show an RMS spread of the response of

- $(1.3 \pm 0.4)\,\%$, when no integrator calibration is applied
- $(0.95 \pm 0.30)\,\%$ with integrator calibration taken into account. The responses given in Table 1 should be multiplied by the respective calibration factor.

After the integrator calibration is considered, the expected RMS spread is the same as in the case of a single module, since the same sources of uncertainties contribute.

The RMS spread found with data $(0.95 \pm 0.30)\,\%$ still matches the expected one ($0.65\,\%$) within errors.[7)] On the other hand, the difference might indicate that another source of uncertainties was not yet considered.

5.2 Pion response versus energy

This Section summarizes the results on the pion response as a function of the beam energy. Data from various modules at a fixed impact angle of $|\eta| = 0.35$ were analyzed.

Data taken with Tilecal modules do not provide a broad energy scan in any single module; instead, data taken with any particular module typically span only two or three energies. Therefore when studying the response to pions vs. energy the module-to-module variation (see Section 5.1) partially obscures the variation with energy. Since most of the modules were exposed to 180 GeV beam at $|\eta| = 0.35$, the problem can be alleviated by normalization of all modules to a common response at this energy and impact angle. The average of 180 GeV pion responses over all modules studied was chosen as the

[7)] The rather large error is due to limited statistics for which the integrator calibration has been recovered.

common value. When this is done a smoother series of response values is obtained, comprising 6 values in the nominal beam energy range from 10 GeV to 350 GeV.

All available pion results at $|\eta| = 0.35$ are summarized in Fig. 9 and Table 2. Figure 9, left panel, compares the measured responses with the MC simulations. They are in reasonably good agreement with experimental data. After normalizing the response of each module at each energy to the common response at 180 GeV, the remaining error on each single response measurement is estimated to be 1 %. It mostly arises from variations in local module response, uncertainties in the charge injection and the cesium calibration (see also Section 5.1.1). This error is combined in quadrature with the uncertainty in the beam energy.

The experimental data are further corrected for longitudinal (see Appendix C) and transverse energy leakage. The latter corrections are necessary, in particular because the pion response is summed from cells of a cone $R \approx 0.2$ as mentioned in Section 3. Two sets of transverse leakage corrections were calculated: from the GEANT4 MC simulations[8)] and from a study of transverse leakage performed on data from Tilecal prototype modules [9]. While GEANT4 simulations are known to underestimate the transverse leakage fraction [10], the latter studies may be an overestimate because of the greater radial depth of the prototype modules. The averages of the two correction factors were used to correct the responses for each beam energy. The systematic error equal to one-half the difference between the two sets of corrections is added in quadrature to the uncertainties described above.

The corrected pion response slowly raises with energy as expected for a non-compensating calorimeter. It obeys the formula

$$\frac{E(\pi)}{E_{\text{beam}}} = (1 - F_{\text{h}}) + F_{\text{h}} \times \left(\frac{\text{e}}{\text{h}}\right)^{-1} \tag{5}$$

where e/h is the ratio of the response to purely EM and hadronic components of showers. The fraction of the non-EM component F_{h} of pion-induced showers with the incident energy E_{beam} is parametrized according to Groom [11, 12] as

$$F_{\text{h}} = \left(\frac{E_{\text{beam}}}{E_0}\right)^{m-1} \tag{6}$$

where E_0 is the energy at which multiple pion production becomes significant and the parameter m must be determined empirically for a given calorimeter. Among the three free parameters of formulae (5) and (6) the value of E_0 was fixed to 1 GeV. The resulting fit gives the values $\text{e}/\text{h} = 1.33 \pm 0.06 \pm 0.02$ and $m = 0.85 \pm 0.03 \pm 0.01$, see also Fig. 9, right panel. The first error is statistical and the second corresponds to the systematic error on the transverse leakage corrections.

Fitting to the data another commonly used parametrization of the hadronic fraction

$$F_{\text{h}} = 1 - 0.11 \times \log(E_{\text{beam}}/E_0) \tag{7}$$

with E_0 fixed to 1 GeV, the value $\text{e}/\text{h} = 1.336 \pm 0.013 \pm 0.005$ is obtained.[9)] This result on e/h is in agreement with earlier Tilecal measurements [13, 14].

[8)] The setup with 5 barrel modules in a stack was used for this special MC study.

[9)] First error is statistical, the second one is systematics associated with the two transverse leakage corrections. Errors are smaller than in the case of the fit proposed by Groom (6) due to different number of free parameters.

E_{beam} (GeV)	$E(\pi)/E_{\mathrm{beam}}$		Leakage corrections		
			Longitudinal	Transverse	
	Data	GEANT4		GEANT4	Prototypes
10	0.794 ± 0.021	0.768 ± 0.002	1.008	1.012	1.023
20	0.825 ± 0.012	0.820 ± 0.002	1.011	1.008	1.016
50	0.849 ± 0.010	0.858 ± 0.002	1.014	1.006	1.011
100	0.858 ± 0.006	0.871 ± 0.001	1.017	1.006	1.008
180	0.861 ± 0.005	0.878 ± 0.001	1.021	1.005	1.006
350	0.874 ± 0.010	0.884 ± 0.001	1.026	1.004	1.004

Table 2: The pion response relative to the beam energy $E(\pi)/E_{\mathrm{beam}}$, where the responses of every module are normalized to a single value at 180 GeV. Also given is the prediction by GEANT4.8.3 MC using the QGSP and Bertini cascade models. The longitudinal leakage corrections are from Ref. [10]. The corrections for transverse energy leakage were obtained from the same GEANT4 MC and from experimental data of an earlier generation of Tilecal modules [9].

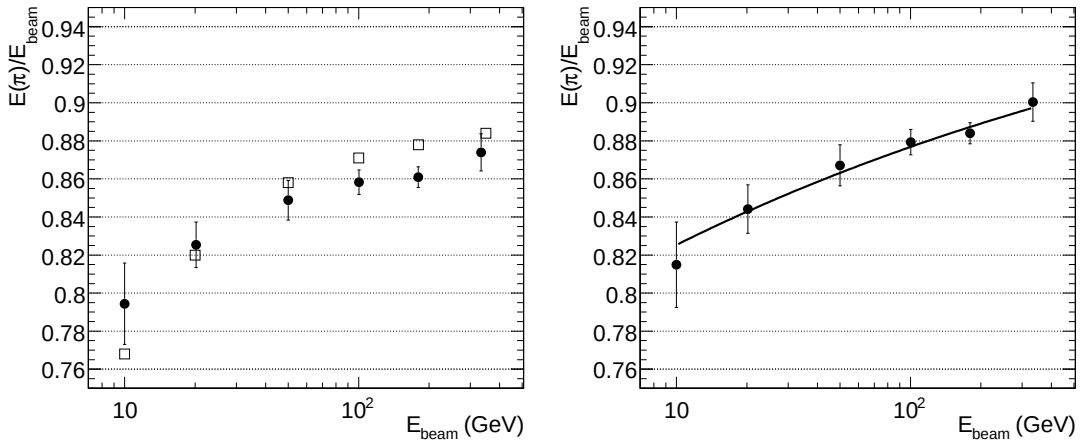

Figure 9: Pion response vs. energy of incident pions at $\eta = 0.35$. Left panel: experimental data (full circles), where the responses in every module are normalized to a single value at 180 GeV. Open squares represent GEANT4 MC simulations. Right panel: the same experimental data corrected for longitudinal and transverse energy leakage, as described in the text. The line shows a fit with the formula (5) using the fraction of the hadronic component as proposed by Groom (6).

E_{beam} (GeV)	Resolution σ/E (%)		
	measured	noise contribution	measured, noise subtracted
10	17.7 ± 0.4	1.92 ± 0.18	17.6 ± 0.4
20	13.2 ± 0.3	0.91 ± 0.09	13.2 ± 0.3
50	9.3 ± 0.2	1.12 ± 0.06	9.2 ± 0.2
100	7.8 ± 0.4	0.84 ± 0.02	7.8 ± 0.4
180	6.8 ± 0.3	0.48 ± 0.03	6.8 ± 0.3
350	6.5 ± 0.2	0.28 ± 0.02	6.5 ± 0.2

Table 3: The measured fractional energy resolution for pions and the corresponding total electronic noise contribution for different nominal beam energies. The electronic noise contribution is negligible. Last column shows the measured energy resolution after the noise contribution is subtracted.

5.3 Pion energy resolution

The same data sets used to obtain the pion response (see Section 5.2) are also used to measure the fraction energy resolution as a function of energy. The values are shown in Fig. 10 along with GEANT4 MC simulations. A good agreement is observed.

Before the energy resolution is parametrized in the usual way, let us investigate the electronic noise contribution. Tilecal uses bi-gain readout electronics and each gain exhibits a different electronic noise, typically 18 MeV in high-gain and 0.4 GeV in low-gain respectively. Therefore, the total electronic noise depends on the share of the high- and low-gain channels, which in turn depends on the incident pion energy. The noise was investigated with the special calibration pedestal runs, where both gains are simultaneously recorded. With these special runs, the total electronic noise histograms were constructed on the event-to-event basis using the share of high- and low-gain channels known from the analyzed physics runs.

The results are summarized in Table 3. The total electronic noise is negligible with respect to the measured energy resolution. Therefore, the energy resolution can be parametrized with the usual formula

$$\frac{\sigma}{E} = \frac{a}{\sqrt{E_{\text{beam}}}} \oplus b \tag{8}$$

using only the sampling (stochastic) term a and the constant term b. The fit is shown in Fig. 10 and results in $a = (52.9 \pm 0.9)\,\%/\text{GeV}^{1/2}$, $b = (5.7 \pm 0.2)\,\%$.

The fit (8) was also applied to the measured energy resolution after the noise subtraction (see Table 3) for completeness. It gives the same values of parameters a, b as above ($a = (52.6 \pm 0.9)\,\%/\text{GeV}^{1/2}$, $b = (5.7 \pm 0.2)\,\%$).

Let us compare the results on energy resolution with that obtained in earlier measurements with Tilecal prototype modules [9]. Prototype modules were longer by $1.4\lambda_{\text{I}}$ at $\eta = 0$, therefore hadronic showers were better contained there. Hence, the energy resolution obtained with prototypes is better especially at high energies, as demonstrated in Table 4.

The measurements performed in the 90° configuration also allowed to study the impact of the effective calorimeter length on the energy resolution [10]. Using these results, one can derive the factor that scales the energy resolution from the prototype module length (data taken at incident angle 20°, effective calorimeter length $9.3\lambda_{\text{I}}$) to that of production module (data taken at $|\eta| = 0.35$, effective calorimeter length $7.9\lambda_{\text{I}}$), see Ref. [15]. After scaling the energy resolution measured in prototype modules to the

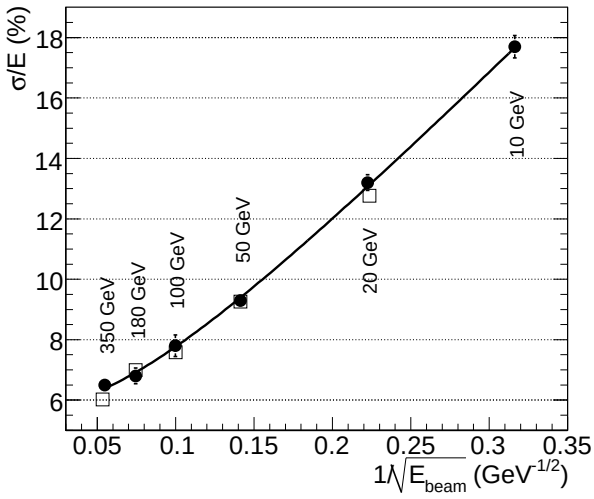

Figure 10: The fractional energy resolution for pions at $|\eta| = 0.35$ as a function of incident energy. Experimental data (full circles) and GEANT4 MC simulations (open squares) are in good agreement. The data are fitted with the usual parametrization (8).

E_{beam} (GeV)	Measured energy resolution (%)		Resolution scaling factor $7.9\lambda_{\mathrm{I}}/9.3\lambda_{\mathrm{I}}$	Prototypes σ/E (%) scaled to $7.9\lambda_{\mathrm{I}}$
	Production modules	Prototypes		
20	13.2 ± 0.3	13.2 ± 0.2	1.022	13.5 ± 0.2
50	9.3 ± 0.2	9.2 ± 0.2	1.057	9.7 ± 0.2
100	7.8 ± 0.4	6.9 ± 0.2	1.097	7.6 ± 0.2
180	6.8 ± 0.3	5.5 ± 0.2	1.148	6.3 ± 0.2

Table 4: The fractional energy resolution for pions measured with production modules (impact angle $|\eta| = 0.35$, effective calorimeter length $7.9\lambda_{\mathrm{I}}$) and with prototype modules [9] (incident angle 20°, effective calorimeter length $9.3\lambda_{\mathrm{I}}$). Also given is the factor corresponding to the ratio of the energy resolution at the two different calorimeter lengths [10,15]. Last column shows the fractional energy resolution measured with prototype modules scaled to the production module length, to be compared with experimental results given in the second column.

length of the production modules, the two resolutions match reasonably well within errors, see Table 4.

6 Conclusions

The uniformity of the response was addressed with 180 GeV hadron beams. The observed response variation reasonably agrees with expectations due to uncertainties in the calibration procedure and local variations in the Tilecal optics system.

The pion response and energy resolution were investigated over the energy range from 10 GeV to 350 GeV. The pion response relative to the incident energy slowly increases with the beam energy as expected for a non-compensating calorimeter; after correction for longitudinal and transverse energy leakage the ratio e/h was determined. The value is in agreement with previous Tilecal measurements. The energy resolution was parametrized with the usual formula and agrees well with the earlier results

obtained with Tilecal prototype modules after accounting for different lengths of the two calorimeters. Both the pion response and the energy resolution were compared to GEANT4 MC simulations, a reasonably good agreement was found.

Acknowledgements

Authors want to express their gratitude to Tancredi Carli, Matteo Cavalli-Sforza, Ana Henriques and Margar Simonyan for many discussions and useful hints. We also want to thank Ilya Korolkov for the discussion on the integrator calibration and Nicolas Kerschen for providing the calculations of precise values of the beam energy settings.

We acknowledge the support from the following funding agencies: Ministry of Education, Youth and Sports of the Czech Republic (projects No. LA08032 and MSM0021620859); Department of International Science and Technology Cooperation, Ministry of Education of the Slovak Republic; Ministerio de Ciencia y Innovación, Spain.

A Testbeam periods

The following modules were used during the respective testbeam periods. Modules are described with their serial production numbers – JINR-XX (barrel modules) and IFA-XX, ANL-XX (extended barrel modules, they are listed in the order EB+, EB−). Also given are beams with their nominal energies and polarities.

June 2002: JINR-34, IFA-59, ANL-8: $-20, +180$ GeV hadrons, $-20, +100, +180$ GeV electrons,

July 2002: JINR-55, IFA-42, ANL-44: $+100, +180$ GeV hadrons, $-10, -20, +50, +100, +180$ GeV electrons,

August 2002: JINR-01, IFA-09, ANL-27: $-10, -20, +180$ GeV electrons,

July 2003: JINR-27, ANL-30, IFA-27: $+100, +180, -350$ GeV hadrons, $+100, +180$ GeV electrons,

August 2003: JINR-63, JINR-13: 180 GeV electrons.

A.1 Bad components

Bad components that occurred during testbeam periods:

- June 2002
  - B+ PMT 17 (cell BC4)
  - EB+ PMT 3 (cell D4)
  - M0− PMTs 2, 4, . . . , 24 for RUN $>$ 200412
  - EB− PMT 10 (cell B-11) for RUN $>$ 200527

  - Side $\eta > 0$ could not be used since the whole module M0+ was not working.

- July 2002
  - M0− PMTs 7, 8, ..., 12 (cells A-2, BC-2, A-3, BC-3) for 100 GeV beam
  - B+ PMT 11 (cell A3), PMT 38 (cell A9)
  - Side $\eta > 0$ could not be used since the whole module M0+ was not working.

- August 2002
  - B− PMT 26 for RUN $>$ 220600 (cell D-2)
  - B− PMT 22 for RUN $<$ 220700 (cell BC-5)

- July 2003
  - B+ PMT 9 (cell A2)
  - M0− PMT 39 (cell A-9)

- August 2003
  - No bad PMTs in the $\eta < 0$ side.

A bad PMT is compensated by using the other PMT of the affected cell twice. Note that there is no way to compensate M0− PMTs 7, 8, ..., 12[10)]. Therefore, data was excluded from analysis if the beam hit the side $\eta < 0$ where the half of barrel module 0 was not working properly.

B Region for signal reconstruction

As already mentioned in Section 3, the signal is summed from cells that correspond to a 3×3 tower matrix. However, the typical testbeam setup includes two extended barrel modules in the top, therefore the 3×3 tower definition is not entirely obvious. In the extended barrel modules, all cells within $|\Delta\eta| < 0.15$ from the beam axis are considered in the sum. The list of extended barrel module cells taken into account for the given pseudorapidity includes:

$\eta = 0.05$: A12, B11, C10, D-4, D4, D5

$\eta = 0.15$: A12, A13, B11, B12, C10, D4, D5

$\eta = 0.25$: A12, A13, B11, B12, C10, D5

$\eta = 0.35$: A12, A13, A14, B11, B12, B13, D5, D6

$\eta = 0.45$: A13, A14, B12, B13, B14, D5, D6

$\eta = 0.55$: A13, A14, A15, B13, B14, D5, D6

$\eta = 0.65$: A14, A15, B13, B14, B15, D6

$\eta = 0.75$: A15, A16, B14, B15, D6

[10)] Both PMTs of cells BC2, A3 are bad.

E_{beam}	$\Delta E/E$ (%)	
	Formula (9)	Formulae (10), (9)
10	n/a	**0.66**
20	**0.84**	0.87
50	**1.26**	1.25
100	**1.69**	1.65
180	**2.06**	2.08
350	n/a	**2.66**

Table 5: The longitudinal energy leakage corrections for $\eta = 0.35$ calculated in two slightly different ways. Second column represents a direct application of the formula (9), while the numbers in the third column were derived with the energy parametrization (10) and then rescaled to the respective calorimeter length by fitting the function (9). Numbers given in bold were used as the final longitudinal leakage corrections, see also Table 2.

$\eta = 0.85$: A15, A16, B14, B15, D6

Cells C10 and D4 are the so-called ITC-cells.

C Longitudinal leakage corrections

The longitudinal leakage corrections for peak response, as determined with a Gaussian fit, were measured in 90° configuration for energies ranging from 20 to 180 GeV [10]. For each beam energy, the leakage is parametrized as a function of the calorimeter length x:

$$\frac{\Delta E}{E} = A \times e^{-x/B} \tag{9}$$

Using the parameters A, B, the longitudinal energy leakage was evaluated by considering the total calorimeter length[11] of 153 cm at $\eta = 0$ that was then scaled to the corresponding impact angle.

For energies 10 and 350 GeV (in this case, the real beam energy was 333.5 GeV, which is taken into account in the energy leakage calculation), the leakage corrections were extrapolated using the energy leakage parametrization as a function of beam energy E_{beam}:

$$\frac{\Delta E}{E} = a \times (E_{\mathrm{beam}})^b \tag{10}$$

Parameters a, b are are given for several calorimeter lengths [10]. Therefore, we have extrapolated the leakage corrections for those lengths using the formula (10). The final leakage correction for the specific calorimeter length was then obtained by applying the fit (9) to energy leakage results of the previous step. This procedure was tested also for energies in the range of 20 to 180 GeV. The two results are in very good agreement, as can be seen in Table 5.

The longitudinal leakage corrections for the 180 GeV hadron response as a function of pseudorapidity were calculated in the similar way, i.e. also using the parametrization (9). However, the beam contains the mixture of pions and protons whose hadronic showers have in principle slightly different longitudinal

[11] Including 1 cm thick frontplate.

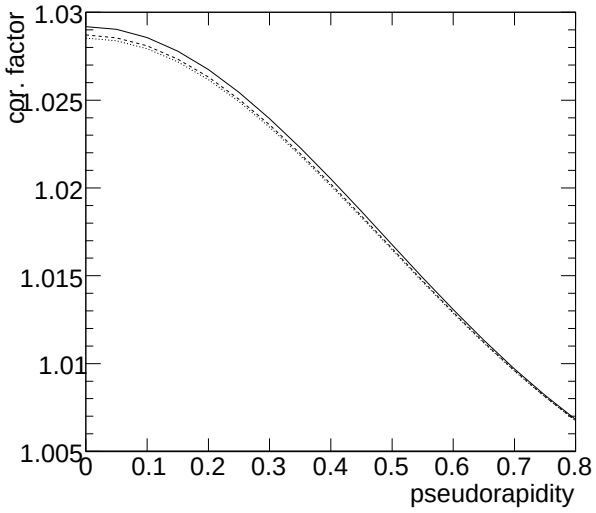

Figure 11: The correction factors for longitudinal leakage for 180 GeV pions (full line), protons (dotted line) and the expected beam composition (dashed line) as obtained from the parametrization given in Ref. [10].

profile. The leakage corrections were therefore calculated both for pure pion and pure proton beam using the parameters A, B listed in Ref. [10] and also for the expected beam composition (26 % pions, 74 % protons at this beam energy). The results are shown in Fig. 11. The difference between the longitudinal leakage corrections for pions and protons is very small at this beam energy. The correction calculated for the expected beam composition was finally used to correct data in Fig. 7.

References

[1] Anderson, K J; Batkova, L; Cavalli-Sforza, M; Carli, T; Cascella, M; Davidek, T; Del Prete, T; Djobava, T; Dotti, A; Febbraro, R et al., *Calibration of ATLAS Tile Calorimeter at Electromagnetic Scale*, ATL-TILECAL-PUB-2009-001 (2009), ATLAS Note.

[2] Anderson, K J; Hurwitz, M H; Jen-La Plante, I; Pilcher, J E; Teuscher, R, *Performance and Calibration of the TileCal Fast Readout Using the Charge Injection System*, ATL-TILECAL-INT-2008-002 (2008), ATLAS Internal Note.

[3] Simonyan, M, *Electron-pion separation in the ATLAS Tile hadron calorimeter*, ATL-TILECAL-PUB-2006-003 (2006), ATLAS Note.

[4] Fredriksson, S. and Eilam, G. and Berlad, G. and Bergström, L., *High-energy collisions with atomic nuclei: The experimental results*, Physics Reports 144 (1987) 187–320.

[5] Kerschen, N, *private communication*, (2007).

[6] Agostinelli S, et al, Nucl. Instr. and Meth. A 506 (2003) 250.

[7] Allison J, et al, IEEE Trans. Nucl. Science 53 (2006) 270.

[8] Hurwitz, M, *Module-to-module uniformity at 180 GeV in 2002–2003 TileCal calibration testbeams*, ATL-TILECAL-PUB-2006-008 (2006), ATLAS Note.

[9] Volpi, M; Cavalli-Sforza, M, *Reanalysis of the Response of 95 Prototype Modules*, ATL-COM-TILECAL-2008-019 (2008), ATLAS Note.

[10] Hakobyan, H; Simonyan, M; Carli, T; Henriques-Correia, A M, *Measurement of Pion and Proton Longitudinal Shower Profiles up to 20 Nuclear Interaction Lengths with the ATLAS Tile Calorimeter*, ATL-TILECAL-PUB-2007-008 (2006), ATLAS Note.

[11] Gabriel T A, Nucl. Instr. and Meth. A 338 (1994) 336.

[12] Groom D E, Nucl. Instr. and Meth. A 572 (2007) 633.

[13] ATLAS Tilecal collaboration, *ATLAS Tile Calorimeter Technical Design Report*, CERN/LHCC/96-42 (1996).

[14] Amaral P; et al, Nucl. Instr. and Meth. A 443 (2000) 51.

[15] Carli, T and Simonyan, M, *Resolution and longitudinal leakage from 90 deg data*, talk given at Tilecal Pion Taskforce meeting, CERN, 31.10.2007.